Supermodeled sabercat, predatory behavior in *Smilodon fatalis* revealed by high-resolution 3D computer simulation

Colin R. McHenry*[†‡§], Stephen Wroe[†], Philip D. Clausen*, Karen Moreno[†], and Eleanor Cunningham[¶]

*School of Engineering and [‡]School of Environmental and Life Sciences, University of Newcastle, Callaghan, NSW 2308, Australia; [†]School of Biological, Earth and Environmental Sciences, University of New South Wales, Sydney, NSW 2052, Australia; and [¶]Newcastle Mater Misericordiae Hospital, Edith Street, Waratah, NSW 2298, Australia

Edited by J. Thomason, University of Guelph, Guelph, Canada, and accepted by the Editorial Board August 16, 2007 (received for review June 28, 2007)

The American sabercat *Smilodon fatalis* is among the most charismatic of fossil carnivores. Despite broad agreement that its extraordinary anatomy reflects unique hunting techniques, after >150 years of study, many questions remain concerning its predatory behavior. Were the "sabers" used to take down large prey? Were prey killed with an eviscerating bite to the abdomen? Was its bite powerful or weak compared with that of modern big cats? Here we quantitatively assess the sabercat's biomechanical performance using the most detailed computer reconstructions yet developed for the vertebrate skull. Our results demonstrate that bite force driven by jaw muscles was relatively weak in *S. fatalis*, one-third that of a lion (*Panthera leo*) of comparable size, and its skull was poorly optimized to resist the extrinsic loadings generated by struggling prey. Its skull is better optimized for bites on restrained prey where the bite is augmented by force from the cervical musculature. We conclude that prey were brought to ground and restrained before a killing bite, driven in large part by powerful cervical musculature. Because large prey is easier to restrain if its head is secured, the killing bite was most likely directed to the neck. We suggest that the more powerful jaw muscles of *P. leo* may be required for extended, asphyxiating bites and that the relatively low bite forces in *S. fatalis* might reflect its ability to kill large prey more quickly, avoiding the need for prolonged bites.

biomechanics | finite element analysis | paleobiology | Pleistocene

That the saber-toothed cat *Smilodon fatalis* was a predator of relatively large mammalian prey is almost universally agreed upon, but how it may have caught and killed animals such as mammoth, bison, and horses remains the subject of one of paleontology's longest-running debates (1–14). In the first attempts to reconstruct the sabercat's biology, it was proposed that the upper canines were used to penetrate hide in a "stabbing" action (2, 3) involving forces generated by the neck muscles (4). Some further suggested that prey were bitten only after being restrained by the powerful forelimbs (15). Consideration of canine morphology led some to interpret the sabers as "slashing" tools and the sabercat as a scavenger (5). Underpinning many of these early interpretations were assertions that the sabercat's bite force was low compared with that of large conical-toothed felids because of reduced jaw muscle and inlever dimensions (2).

Consensus has grown around active predation and the canine-shear-bite hypothesis (6), which holds that opposition from the lower canines allowed the upper canines to puncture prey tissues. However, questions surrounding bite force and relative contributions of cranial and cervical musculature remain contentious, as does the question of whether *S. fatalis* bit at the neck or belly of prey (6, 7, 10–14). Considerations of mandibular anatomy, muscle scarring, and possible mechanical advantage imparted by a wider gape have suggested that contrary to earlier interpretations, cranially generated bite forces were high (10–12, 16), but, consistent with earlier arguments (2), bite force predictions based on cross-sectional area (CSA) of muscle indicate that bite force was low for such a large cat (13, 14).

A recent numerical analysis, using 2D beam modeling, of the mandibles in a range of felids suggested that the lower jaw of saber-toothed cats was not mechanically optimized to resist the forces resulting from struggling, unrestrained prey (12). The same analysis also suggested high mechanical strength in saber-toothed cat mandibles relative to mandibular length, and hence inferred high bite forces. However, the lower jaw of *S. fatalis* is shorter relative to skull length than that of an African lion, and it is even smaller still if scaled for body mass [supporting information (SI) Table 1]. The effects of scaling relationships and 3D geometry in comparing saber-toothed with conical-toothed felids remain hitherto unexplored.

To further address killing behavior in *S. fatalis*, we have developed new protocols that facilitate realistic 3D computer-based simulation of the vertebrate skull using a finite element (FE) approach (17, 18). This represents the first FE analysis of a fossil carnivoran. Improvements over previous FE analyses of the vertebrate skeleton (19–22) include (*i*) higher model resolution (>1.8 million elements), (*ii*) incorporation of the variable, heterogeneous material properties of bone to more realistically simulate mechanical behavior (23) (SI Fig. 5), (*iii*) treatment of the cranium and mandible as an articulated unit, (*iv*) 3D reconstruction of the jaw musculature (Fig. 1), and (*v*) simulation of cervical musculature (Fig. 1*B* and SI Fig. 6).

The lack of data for *in vivo* bite force and material properties for bone in living felids disallows calculation of strict performance limits and underscores the need for comparative treatment (22, 24). Our analysis is founded in simulations of both *S. fatalis* and a large living felid, *Panthera leo* (lion) (Fig. 1). We assessed relative mechanical performance on the basis of mean stress and strain for the crania and mandibles (Fig. 2), as well as visual output of the postprocessing software (Figs. 3 and 4). Models assuming a single (homogeneous) material property (Fig. 2) and hypothetical nonuniform values provided basic sensitivity analyses (SI Fig. 7).

Loads relating to (*i*) muscle forces generated by the jaw adductors and head flexors ("intrinsic") or (*ii*) to movement of prey relative to the predator (25) ("extrinsic") were applied. The

Author contributions: C.R.M., S.W., and P.D.C. designed research; C.R.M., S.W., and E.C. performed research; C.R.M., S.W., P.D.C., K.M., and E.C. contributed new reagents/analytic tools; C.R.M., P.D.C., K.M., and E.C. analyzed data; and C.R.M. and S.W. wrote the paper.

The authors declare no conflict of interest.

This article is a PNAS Direct Submission. J.T. is a guest editor invited by the Editorial Board.

Abbreviations: CSA, cross-sectional area; CT, computed tomography; FE, finite element.

[§]To whom correspondence and requests for materials should be addressed. E-mail: colin.mchenry@newcastle.edu.au.

This article contains supporting information online at www.pnas.org/cgi/content/full/0706086104/DC1.

www.pnas.org/cgi/doi/10.1073/pnas.0706086104

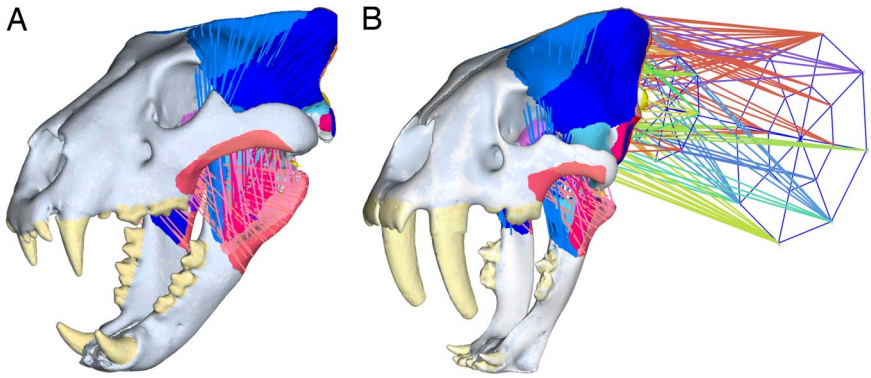

Fig. 1. Construction of models. (*A*) Lion model showing the Temporalis (blue) and Masseter (red) systems muscle ''beams'' and attachment areas. (*B*) *S. fatalis* model showing the neck assembly. The different colored beams on the neck correspond to neck muscle groups in felids. Note that the upper canines of the *S. fatalis* model are based on restored teeth in the scanned specimen (see *SI Text*), and they are included in the model to provide accurate geometry for bite forces rather than an assessment of the stresses and strains acting upon these teeth.

potential advantage imparted by gape was factored into the models. Muscle forces were calculated by using 2D techniques (13, 26, 27) refined for 3D models. Loads were designed to address the following questions. How well equipped was *S. fatalis* to resist extrinsic loads generated by unrestrained prey? Are calculated mechanical responses of the sabercat to jaw adduction consistent with interpretations of low or high cranially driven bite force compared with extant cats? Could *S. fatalis* have maximized available bite force by recruiting cervical musculature? Does the skull respond differently to a puncture (''canine-shear'' or ''stab'') bite as opposed to ''pull-back'' (mechanically equivalent to ''cut-and tear,'' ''slash,'' or ''slice'' hypotheses) retractive loadings?

These questions were assessed against the performance of the lion model under equivalent loadings. *Panthera leo* is known to bite relatively large, unrestrained prey (28); has near ''typical''

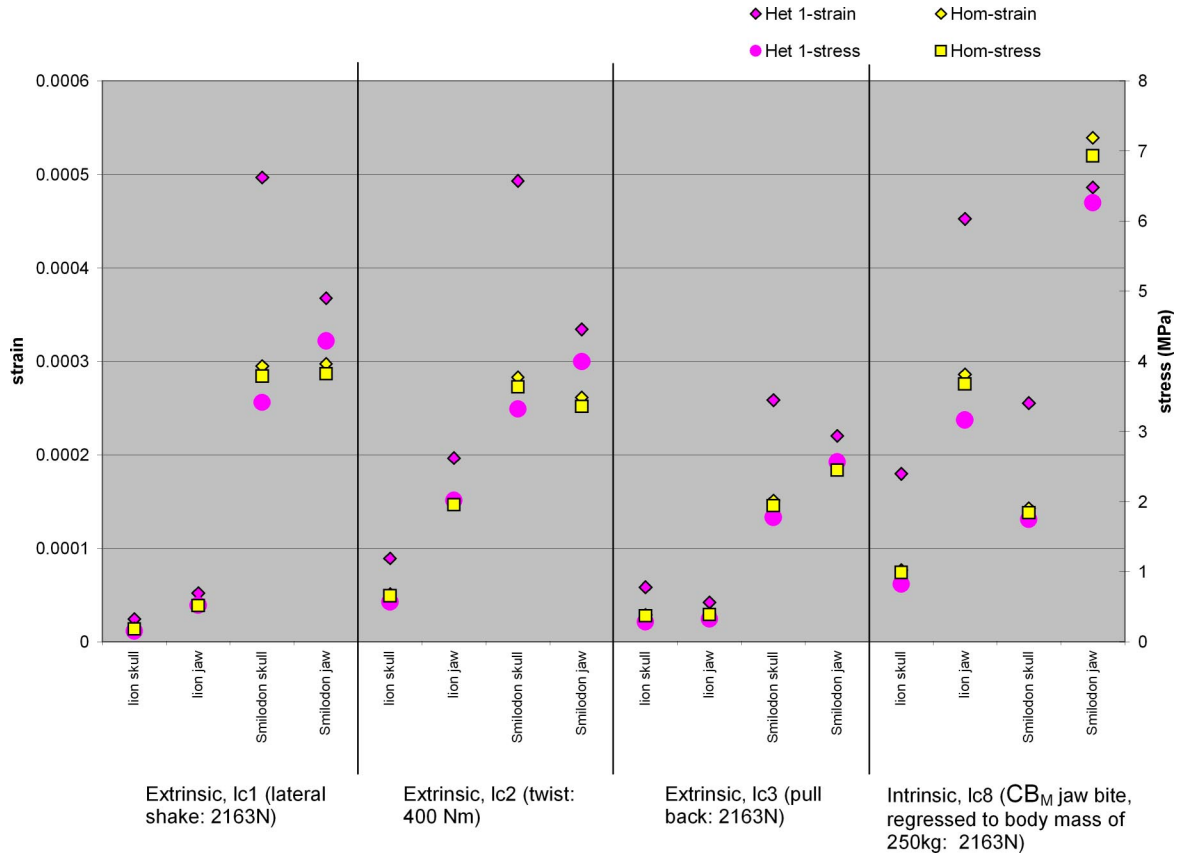

Fig. 2. Mechanical performance of *P. leo* and *S. fatalis* heterogeneous (Het) and homogeneous (Hom) models under extrinsic and intrinsic loads, plotted as mean brick Von Mises stress and strain for skull and mandible. For extrinsic loads, load case 1 (lc1) is a laterally directed force of 2,000 N, load case 2 (lc2) is a 100,000-Nmm moment applied around the anterior–posterior axis, and load case 3 (lc3) is an anteriorally directed 2,000-N force, all applied to the canines. Note that, for the purposes of visual comparison, results for the intrinsic loads are for a cranially driven bite and for each model are scaled to the average bite force of a 250-kg felid (2,163 N), whereas extrinsic forces in lc1 and lc3 (originally 2,000 N) have been scaled to those plotted for intrinsic forces (2,163 N). Torsional loads (extrinsic, lc2—originally 100,000 Nmm) have been scaled by 4 so that the results are of the same order as those for the forces.

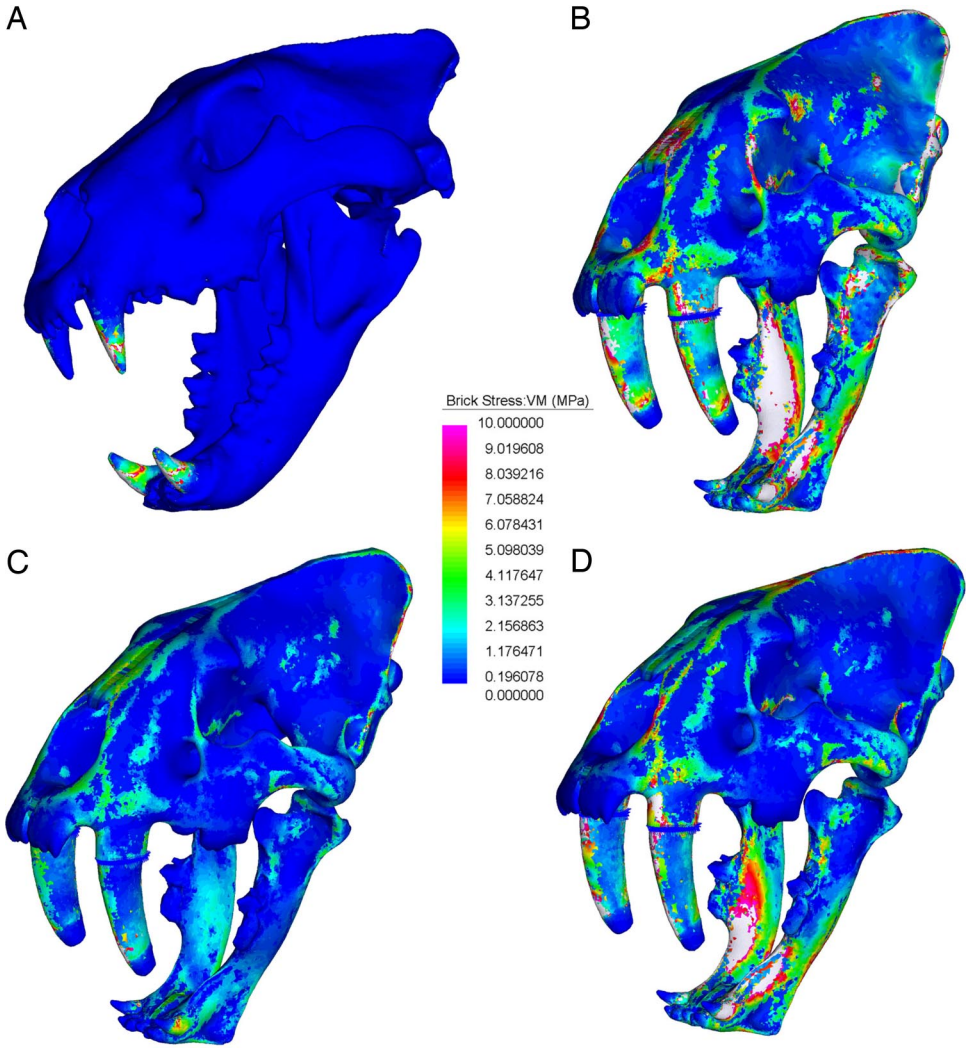

Fig. 3. Von Mises stress under extrinsic loads. The models are subjected to various loads applied to the canines. Jaw and neck ''muscles'' are used to brace the skull but do not apply forces. (*A*) Lion with 2,000-N lateral force (extrinsic load case 1: lateral shake). (*B*) *S. fatalis* with 2,000-N lateral force (extrinsic load case 1). (*C*) *S. fatalis* with 100-Nm axial moment (extrinsic load case 2: twist). (*D*) *S. fatalis* with 2,000-N anterior force (extrinsic load case 3: pull-back). Note that the stresses shown on the restored upper canines of the *S. fatalis* model are artificial (see *Materials and Methods* and *SI Text*).

bite force for a conical toothed felid of its body mass (13); is not particularly reliant on head flexing musculature to produce bite force [cervical musculature may play some role in bite force generation for all cats (11)]; and generally uses a prolonged ''clamp-and-hold'' bite to kill large prey (28, 29).

Results

We found that under laterally directed extrinsic loads, mean ''brick'' element stress and strain were much greater in the *S. fatalis* skull than in the lion's (Fig. 2). Qualitative patterns for this and all other load cases were similar for heterogeneous and homogeneous models, and were consistent with surface plots of mean brick stress (Fig. 3 *A* and *B*). Mean stress and strain in the sabercat model were closer to, but greater than, the lion values under torsional extrinsic loads. These differences were particularly notable in surface plots for lateral loading (Fig. 3 *A* and *B*). Biting large unrestrained prey exposes cats to higher lateral or torsional forces (11). Our modeling shows that the sabercat's skull is less well adapted for such a role than is the lion's.

Under intrinsic loads, mean stresses and strains in the mandible greatly exceed those of the cranium for both models. Stress and strain in the *S. fatalis* cranium and mandible exceed the respective levels in the lion model. Again, these results hold qualitatively for both heterogeneous and homogeneous models, and they are consistent with previous suggestions that the mandible is of particular mechanical importance during jaw adduction (25). Surface plots of both models suggest that stress is especially high at the coronoid process and zygomatic arch, areas of jaw muscle attachment. The mandibular ramus of *S. fatalis* also carries high stress (Fig. 4 *A* and *B*).

Heterogeneous modeling highlights an interesting feature of the sabercat's mandible. Although it carries far greater stresses than the lion's, strain is similar (Fig. 2). Its mandible differs from its own cranium, and the lion's cranium and mandible, in carrying lower strain for a given stress. This is evident across all intrinsic and extrinsic load cases and points to relatively high elastic (Young's) modulus in the sabercat's lower jaws, a finding consistent with observations that the mandible comprises a high proportion of cortical bone (11). This composition may increase strength (in terms of maximum stress carried before yield) of the mandible in *S. fatalis*, but there is a potential cost if yield point is exceeded: Yield in bone is controlled by strain, but yield strain decreases with increasing modulus (30). Additionally, because ultimate strain correlates negatively with mineral content (30),

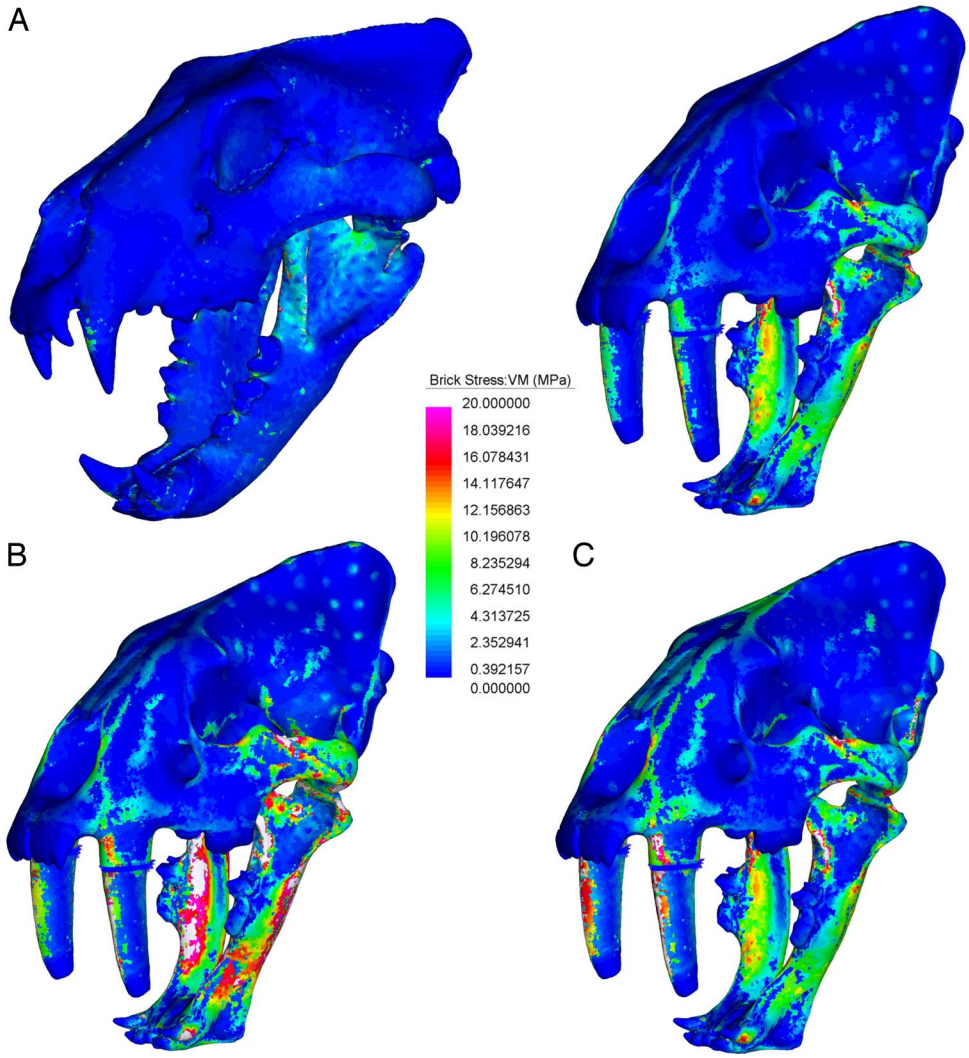

Fig. 4. Von Mises stress under intrinsic loads (bilateral canine bites). (*A*) Bite force predicted by 3D dry skull method, adjusted to account for pennation; shown are lion biting at 3,388 N (*Left*) and *S. fatalis* biting at 1,104 N (*Right*). (*B* and *C*) *S. fatalis* biting at the forces calculated from ref. 13 for the regression of bite force on body mass for a 229-kg felid (2,110 N), powered by jaw adductors only (*B*) and by neck + jaw muscles (*C*).

and mineral content strongly influences modulus, it is possible that once yield strain was exceeded, failure would quickly become catastrophic.

This increase in bone stiffness may be analogous to the morphology of bird and pterosaur bones, where maximum strength is required for minimal weight (31). That mandibular weight was a critical factor for *S. fatalis* is less likely, but if the operation of the skull in sabercats constrained mandibular size, then the increased stiffness may allow a relatively smaller structure to provide relatively greater strength—relative to skull length, mandible size in the sabercat is less than in the lion (SI Table 1). Conversely, very stiff skeletal elements may be more prone to breakage under sudden, peak loads, and the high stiffness of the mandible may be possible only if the mandible played a small role in prey dispatch (1, 16). The latter is consistent with an interpretation of the mandible as being optimized for prey processing bites that benefit from increased stiffness (analogous to man-made cutting tools). Alternatively, these mandibular properties may relate to its use as a strut involving axial compressive loads (6), or may underscore the necessity of prey restraint before biting (12).

Our modeling clarifies questions surrounding resultant bite force in the sabercat. 2D modeling suggests that, when adjusted for body mass, CSA of the jaw adductors was relatively low in *S. fatalis* (13), and calculated bite force is 47% of the lion's (SI Table 2). When we allow for 3D muscle geometry, resultant bite force in *S. fatalis* is relatively lower still (33% of the lion's, SI Table 2), even after accounting for conversion of physical CSA to physiological CSA (26). Because the 2D and 3D methods use the same estimate of jaw muscle force, the differences between them are necessarily a result of differences in estimates of muscle and inlever geometry. The sabercat's small coronoid process (2) may be important here, because it is likely to reduce the mechanical advantage of the temporalis. In load cases where bite force is calculated by 3D methods, surface stress in the lion's skull is lower than the sabercat's, but both are almost entirely below 20 MPa (Fig. 4*A*). However, if jaw adductor force in *S. fatalis* is increased to the level at which resultant bite force equals that predicted for conical-toothed felids of equivalent body mass (2,060 N for a 229-kg felid; SI Tables 1 and 2), surface stress is far greater than in the lion, especially in the mandible (Fig. 4*B*). Because, for a given bite force, the sabercat's cranium carries lower stress than the mandible, raising effective bite force by increasing head flexor rather than jaw adductor force results in lower overall stresses (Fig. 4*C*) than scenarios wherein high bite forces are produced by jaw adductors alone.

Intrinsic load cases produce bite forces largely oriented along the long axis of the canines. In contrast, loads produced during pull-back behaviors impose anteriorally directed forces. The response of the sabercat's skull to these two different load cases is similar for comparable force magnitudes (Fig. 2). However, the results do not allow for differences in the tooth area to be forced through prey tissues: If this is higher for any of the behavioral equivalents of the pull-back load case, greater forces would be required, and stress and strain would exceed the levels seen in simple stabs or bites.

Discussion

Our FE analyses quantitatively demonstrate that the sabercat's skull was not optimized for resisting high, multidirectional loads imposed by unrestrained prey, a finding consistent with interpretations of mandible morphology (12). Its massive size, robusticity, and hypertrophied dew claws (32–34) may have provided it with sufficient force, inertia, and purchase to bring down large animals without biting until the prey was grounded. Large prey are most easily restrained by the head, and we conclude that the killing bite was directed to the neck, a behavior that has also been suggested for the Miocene saber-toothed cat *Paramachairodus* (35).

Similarly, earlier interpretations of relatively low bite force in *S. fatalis* are consistent with our results for stress, especially in the mandible. Whether the force calculated for the jaw adductor bite alone (≈1,100 N) was sufficient for the canines to penetrate thick hide remains unknown. However, it is clear that if the sabercat used a jaw-bite as strong as that of an average felid of equivalent body mass, both the cranium and the mandible would receive far greater stresses. Reconstructions of higher bite forces in *S. fatalis* on the basis of mandibular section (12) do not account for large differences in the mandible's size, relative to the cranium or body mass, between it and extant pantherines (SI Table 1).

If *S. fatalis* required more than a 1,100-N bite force to drive its upper canines through hide, our results suggest that this extra force could have been supplied by the head flexors without stress or strain exceeding levels experienced by the lion mandible during a jaw-bite. Thus, both a jaw- and neck-muscle-driven bite (canine-shear) and an entirely neck-muscle-driven bite (stab) are mechanically feasible. However, we consider the former more likely because it makes more efficient use of available muscle force. Neck-muscle-driven bites have been suggested for *Paramachairodus* on morphological grounds (35). When a 1,104-N jaw adductor bite is complimented by a 956-N neck-driven bite, surface stress does not exceed 20 MPa (Fig. 4*C*).

It has been argued in an explanatory context for the canine-shear-bite model that mandibular strength and jaw-driven bite force in *S. fatalis* were necessarily high (6). However, the actual magnitude of force needed remains unquantified. Regarding the veracity of behavioral models, we suggest that the pressing question is not whether structural strength or bite forces were high or low, but whether they were sufficient to enable behaviors as hypothesized. In the absence of quantitative estimates of forces required by competing hypotheses, our results are currently most consistent with the canine-shear-bite hypothesis.

The impressive mechanical behavior evidenced by our lion simulations also deserves consideration. How might lions deploy such force, and why do they need it? The lion's skull can resist high extrinsic loads, but this need not require that bite forces be applied simultaneously. Killing techniques used by lions can require bites exceeding 13 min (28, 29), but it is unlikely that that maximum force could be sustained over such periods (36). Powerful jaw muscles may reflect a need for sustained rather than high peak bite forces, whereas less powerful jaws in the sabercat may reflect a more rapid kill.

Materials and Methods

Model Construction. Specimens were scanned by computed tomography (CT), and the scan data were imported into STRAND7 FE software (*SI Text* and SI Table 3). Material properties were assigned on the basis of CT attenuation (Heterogeneous and Hypothetical versions) or predetermined values for bone (Homogeneous version) (SI Table 4 and SI Fig. 8).

To simulate the action of the cervical musculature in bracing the skull upon the neck assembly (SI Fig. 6), we used a series of simplified beam elements (122 in the lion model and 128 in the *S. fatalis* model). Topology and relative size of muscles were based on data from ref. 37 for *Felis*. Skull attachments replicated actual attachments closely, and attachments to postcranial elements were matched as closely as possible to the node on the neck frame that corresponded best to the postcranial anatomy; i.e., the posterior attachment of sternomastoideus, which in life is to the manubrium, was to the ventral midline node at the posterior end of the frame (SI Fig. 6). The simulated neck muscles were similar in each model, except for the beams inserting upon the mastoid process; in the *S. fatalis* model, there were 12 beams representing M. sternomastoideus vs. 6 beams in the lion model. We did not model the obliqus capiti system as a separate muscle, but it inserts upon the mastoid adjacent to sternomastoideus and differences in its size between *S. fatalis* and pantherines may be more pronounced than with sternomastoideus and may reflect its importance in head flexion (9, 38). Simulating the cervical musculature to a greater level of detail might slightly alter some force vectors, but it is most unlikely to substantially affect moments or resulting stress patterns, and the level to which we have approximated the cervical muscles is appropriate for the purposes of the model.

For intrinsic bites, all neck muscle beams were assigned a modulus of 0.1 MPa, reflecting the modulus of relaxed muscle (39). For intrinsic neck-powered bites, forces were applied to the beams simulating the head flexors (cleidomastoidus, levator scapula ventralis, longus capitus, longissimus capitus, rectus capitus ventralis, and sternomastoideus).

Modeled thus, the additional bite force resulting from activation of the head flexors was small (72 N) in the lion and somewhat larger (155 N) in *S. fatalis*; however, the cervical musculature may have been proportionately far greater than modeled in the sabercat (8, 9), and for the jaw + neck bite, we increased the bite force component from the head flexors so that the resultant bite force was of the required magnitude.

For extrinsic loads, neck muscle beams were assigned a modulus of 15 MPa, on the basis of data for muscle under contraction (39), providing strong bracing of the head against the load without preventing movement at the neck joint.

For the FE analysis, linear static solves were used. The large model sizes prohibited measurement of statistical means using commercially available software, and these were calculated using code written in RGui programming language by K.M.

Jaw Muscles, Bite Force, and Extrinsic Loads. For each specimen, forces for temporalis and masseter-pterygoid systems were calculated by using the dry skull method (13, 26). This technique provides specimen-specific estimates of force generated by jaw adductors for mammals by measuring physical CSA for each muscle system using 2D skull geometry. Within each muscle system, attachment areas for individual muscles were subdivided following data from ref. 40 on the masticatory muscles of *Felis*. For each muscle, a number of approximately parallel, simplified beam elements connected the origin and insertion areas to simulate the basic geometry of muscle fibers. This method automatically determines force vectors. The number of simplified beams per muscle was adjusted to keep the force per beam within a consistent range (SI Table 5).

When used with 2D skull models, the moment applied to the jaw by the jaw muscles is calculated by assuming that the inlever of each muscle system passes through the centroid of the physical CSA used to derive muscle force. This was then used to calculate the resultant force at a bite point along the tooth row, for example, providing a dry skull estimate of canine bite force (CB_S). When modeled in 3D, jaw muscle moment is approximated by using more realistic muscle attachment geometry, and it provides a more accurate estimate of muscle inlever dimensions and orientation; the resultant bite force is thus calculated as a 3D version of a dry skull estimated canine bite force ($CB_{S\,3D}$), in contrast to the 2D version ($CB_{S\,2D}$).

Muscle forces calculated from physical CSA do not account for the potential increased force production allowed by pennation; for that a measurement of physiological CSA is required. Thomason (26) specified the equation for the relationship between canine bite force as calculated from physical CSA (CB_S) and physiological CSA (CB_M) [$\log_{10}(CB_M) = 0.858 \log_{10} CB_S + 0.559$]. We used this equation to transform calculated $CB_{S\,3D}$ to a figure for $CB_{M\,3D}$, and the scaling factor between the two was used to calculate muscle forces that account for pennation.

For each model, a final estimate of bite force was made on the basis on the regression of body mass to CB_S for felids by using data from ref. 13. This regression provided an estimate of the expected bite force for a typical felid of a given body mass. This figure was adjusted for pennation to provide an estimate of $CB_{M\,REG}$ for each model (SI Table 2).

Bite forces were measured as force resultants acting upon nodes at canine tips, which were restrained in the axis of the jaw joint. To reduce the incidence of artefacts that result from single nodes being restrained, the surface faces of the elements near each canine tip were tessellated with a mesh of stiff beams, allowing the resulting forces to be dissipated more evenly across the surface of the tooth and replicating the effect of a tooth being partially embedded in soft tissues. It is important to note that these linear static analyses simulate the total force applied to the prey but do not simulate cutting of tissues by teeth, and the bite force results are not affected by the fact that the canines in the scanned specimen of *S. fatalis* were restored (see *SI Text*). Although stresses and strains in these restored upper canines do not reflect the actual mechanical performance of real teeth, we assume for the purposes of our analysis that the restored teeth apply loads resulting from the bite to the skull in a realistic manner. To simulate the application of extrinsic loads to the canines, nodes at the canine tip were connected with rigid links, and the relevant load applied to these links. For the lateral shake (load case 1), a force of 2,000 N was applied, directed to the left side. For the twist (load case 2), a moment of 100,000 Nmm was applied about the longitudinal axis of the skull. For the pull-back (load case 3), a 2,000-N force was applied acting forwards from the teeth. Load magnitudes were chosen to lie within the calculated range of bite forces (see above); application of equivalent load magnitudes to each model implies predation upon similarly sized prey.

We thank Bob Callister, Gerard Carè, Jim Cunningham, Mike Habib, Sandy Ingleby, Robert Jones, Edmund Martin, and Atul Pendharkar. Work was funded by Australian Research Council (ARC) Discovery, ARC QE2 Research Fellowship, and University of New South Wales Strategic Research Initiatives grants (to S.W.), and an Internal Grant (University of Newcastle) (to P.D.C.).

1. Miller GJ (1969) *Tebiwa* 12:9–19.
2. Matthew WD (1910) *Bull Am Mus Nat Hist* 28:289–316.
3. Warren JC (1853) *Proc Boston Soc Nat Hist* 4:256–258.
4. Simpson GG (1941) *Am Mus Novit* 1130:1–12.
5. Marinelli W (1938) *Paleobiologica* 6:246–272.
6. Akersten W (1985) *Los Angeles Co Mus Contrib Sci* 356:1–22.
7. Bryant HN (1996) in *Paleoecology and Paleoenvironments of Late Cenozoic Mammals*, eds Steward KM, Seymour KL (Univ of Toronto Press, Toronto), pp 283–299.
8. Anton M, Galobart A (1999) *J Vert Paleontol* 19:771–784.
9. Anton M, Galobart A, Turner A (2005) *Quat Sci Rev* 24:1287–1301.
10. Duckler GL (1997) *J Vert Paleontol* 17:600–609.
11. Biknevicus AR, Van Valkenburgh B (1996) in *Carnivore Behavior, Ecology and Evolution*, ed Gittleman JL (Cornell Univ Press, Ithaca, NY), pp 393–428.
12. Therrien F (2005) *Zool J Linn Soc* 145:393–426.
13. Wroe S, McHenry C, Thomason J (2005) *Proc R Soc London Ser B* 272:619–625.
14. Christiansen P (2006) *J Morphol* 267:1186–1198.
15. Schultz CB, Martin LD (1970) *Bull Univ Nebraska State Mus* 9:33–38.
16. Emerson SB, Radinsky L (1980) *Paleobiology* 6:295–312.
17. Wroe S, Moreno K, Clausen P, McHenry C, Curnoe D (2007) *Anat Rec Part A* 290:1248–1255.
18. Wroe S, Clausen P, McHenry C, Moreno K (2007) *Proc R Soc London Ser B* 10.1098/rspb.2007.0906.
19. Rayfield EJ, Norman DB, Horner CC, Horner JR, Smith PM, Thomason JJ, Upchurch P (2001) *Nature* 409:1033–1037.
20. Snively E, Russell A (2002) *Senckenbergiana Lethaea* 82:35–42.
21. Dumont ER, Piccirillo J, Grosse IR (2005) *Anat Rec Part A* 283A:319–330.
22. McHenry CR, Clausen PD, Daniel WJT, Meers MB, Pendharkar A (2006) *Anat Rec A* 288A:827–849.
23. Thomason JJ (1995) in *Functional Morphology in Vertebrate Paleontology*, ed Thomason JJ (Cambridge Univ Press, Cambridge, UK), pp 249–263.
24. Rayfield EJ (2005) *Zool J Linn Soc* 144:309–316.
25. Preuschoft H, Witzel U (2002) *Senckenbergiana Lethaea* 82:207–222.
26. Thomason JJ (1991) *Can J Zool* 69:2326–2333.
27. Christiansen P, Adolfssen S (2005) *J Zool London* 266:133–151.
28. Schaller GB (1972) *The Serengeti Lion: A Study of Predator-Prey Relations* (Univ of Chicago Press, Chicago).
29. Sunquist M, Sunquist F (2002) *Wild Cats of the World* (Univ of Chicago Press, Chicago).
30. Currey (2004) *J Biomech* 37:549–556.
31. Fastnacht M (2005) *Acta Palaeontol Polonica* 50:273–288.
32. Wroe S, Argot C, Dickman C (2004) *Proc R Soc London Ser B* 271:1203–1211.
33. Christiansen P, Harris JM (2005) *J Morphol* 266:369–384.
34. Cox M, Jefferson GT (1988) *Curr Res Pleistocene* 5:66–67.
35. Salesa MJ, Anton M, Turner A, Morales J (2005) *Zool J Linn Soc* 144:363–377.
36. Enoka RM, Stuart DG (1992) *J Appl Physiol* 72:1631–1648.
37. Crouch JE (1969) *Text Atlas of Cat Anatomy* (Lea & Febiger, Philadelphia).
38. Anton M, Salesa MJ, Pastor JF, Sanchez IM, Fraile S, Morales J (2004) *Zool J Linn Soc* 140:207–221.
39. de Winkel ME, Blange T, Treijtel BW (1994) *J Muscle Res Cell Motil* 15:130–144.
40. Turnbull WD (1970) *Fieldiana Geol* 18:149–356.